Fusion Science and Technology

ISSN: 1536-1055 (Print) 1943-7641 (Online) Journal homepage: https://www.tandfonline.com/loi/ufst20

Design of the Toroidal Field Coil System for the TPM-1U Tokamak

D. Hernández-Arriaga, D. M. Ventura-Ovalle & M. Nieto-Pérez

To cite this article: D. Hernández-Arriaga, D. M. Ventura-Ovalle & M. Nieto-Pérez (2019) Design of the Toroidal Field Coil System for the TPM-1U Tokamak, Fusion Science and Technology, 75:2, 148-159, DOI: 10.1080/15361055.2018.1554390

To link to this article: https://doi.org/10.1080/15361055.2018.1554390

Published online: 12 Feb 2019.

FUSION SCIENCE AND TECHNOLOGY · VOLUME 75 · 148–159 · FEBRUARY 2019

DOI: https://doi.org/10.1080/15361055.2018.1554390

Design of the Toroidal Field Coil System for the TPM-1U Tokamak

D. Hernández-Arriaga,* D. M. Ventura-Ovalle, and M. Nieto-Pérez

CICATA Queretaro – Instituto Politecnico Nacional, Cerro Blanco 141, Queretaro, QRO 76090, Mexico

Received June 5, 2018
Accepted for Publication November 20, 2018

Abstract — *Using infrastructure from the old TPM-1 tokamak in Mexico, there is an ongoing project to bring it back into operation, but with important upgrades. One of the main planned improvements will be the substitution of the continuous winding used to generate the toroidal field (TF) with a set of discrete circular coils. The new toroidal magnetic field configuration should also allow stable operation of the machine at plasma currents of up to 50 kA for 30 ms. At this design stage, decisions regarding number and characteristics of the coils and power delivery strategy to them need to be addressed. In the present paper, a study regarding the parameters required for the generation of the adequate TF are presented, including the process for determining number of TF coils, their size and position, the required current pulse for operation, and a potential strategy for generating such pulse based on passive pulse-forming networks.*

Keywords — *TPM-1 tokamak, toroidal field coil system, pulse-forming networks.*

Note — *Some figures may be in color only in the electronic version.*

I. INTRODUCTION

The TPM-1U tokamak is a small tokamak under construction at CICATA Querétaro. It is based on a four-section toroidal vacuum vessel with 0.45-m major radius and 0.15-m minor radius. Originally, the vessel was designed and constructed more than 20 years ago to study the effect of replacing the set of discrete toroidal field (TF) coils with a continuous wire wound around the toroidal direction[1]; this meant that a small number of ports were present in the vacuum chamber, as can be seen in Fig. 1a. The present port configuration may prove insufficient for placing all the access points required for proper plasma operation and diagnosis. Figure 1b presents the new proposed port configuration for TPM-1U; it is clear that a careful placing of the TF coils will be necessary to avoid port obstructions. Although a large number of coils (and in the limit a continuous toroidal current sheet) give a homogeneous TF, a trade-off between field homogeneity and device access is always necessary.[2]

In order to allow for the realization of an initial scientific program, it is envisioned that the machine needs to have operational parameters in line with currently operating devices of roughly the same size, such as ISTTOK (Ref. 3), GOLEM (Ref. 4), IR-1 (Ref. 5), and STOR-M (Ref. 6). Table I presents the expected parameters to be achieved in the machine in order to keep it comparable with other devices around the world with similar physical dimensions. Other studies by our group have focused on achieving these parameters, such as the design of the pulsed transformer required to achieve the desired plasma current by induction.[7]

II. TOROIDAL MAGNETIC FIELD REQUIREMENTS FOR THE TOKAMAK

II.A. Number, Size, and Position of TF Coils

The first requirement for the TF is homogeneity within the plasma column volume. As mentioned before, a toroidal current sheet (single toroidal turn) would be the only way to achieve a perfectly homogeneous TF, and as the number of TF coils increases, that scenario is approached. Therefore,

*E-mail: daniel_hernandez_arriaga@ieee.org

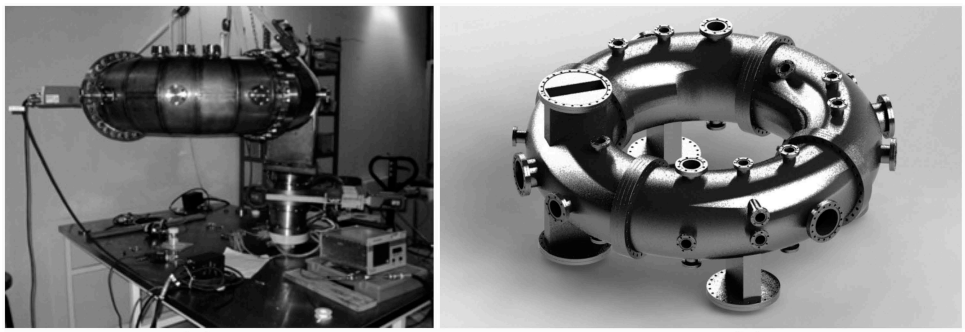

Fig. 1. (a) Photograph of the TPM-1 vacuum chamber and (b) rendering of the proposed new port configuration for the TPM-1U vacuum chamber.

TABLE I

Comparison of Construction and Target Operation Parameters of the TPM-1U Tokamak with Other Devices of Similar Size Around the World

Parameter	GOLEM	ADITYA	ISTTOK	STOR-M	NOVILLO
Major radius (m)	0.4	0.75	0.46	0.46	0.23
Minor radius (m)	0.085	0.25	0.085	0.125	0.06
Central magnetic field (T)	<0.8	1.2	0.5 to 0.6	0.5 to 1.0	0.05–0.47
Plasma current (kA)	<10	80	6 to 11	30 to 60	1 to 12
Central electron density (m^{-3})	3-8 × 10^{19} to 8 × 10^{19}	1 × 10^{19}	1 × 10^{19}	1 × 10^{19} to 3 × 10^{19}	1 × 10^{19} to 2 × 10^{19}
Central electron temperature (eV)	0.6 to 0.8	20 to 500	100 to 250	300	150
Pulse time duration (ms)	<15	60	20 to 60	2 to 5	5

a study regarding field homogeneity given the geometry of the available toroidal chamber is the first step.

As an initial approximation, circular current loops are used to represent each TF coil. By considering the center of the current loop as the origin of a cylindrical (r, z) frame of reference, there are exact expressions for the radial and axial components of the magnetic field normalized to the field at the center of the loop, given by Eqs. (1a) and (1b), respectively[8]:

$$\frac{B_r(r,z)}{B_0} = \frac{\xi}{\rho}\frac{1}{\sqrt{Q}}\left(\frac{2(1+\rho)-Q}{Q-4\rho}E(k)-K(k)\right) \tag{1a}$$

and

$$\frac{B_z(r,z)}{B_0} = \frac{1}{\sqrt{Q}}\left[\frac{Q-2\rho}{Q-4\rho}E(k)+K(k)\right] . \tag{1b}$$

The dimensionless geometric parameters appearing in Eq. (1) are defined as

$$\rho = \frac{r}{R_C} ,$$

$$\xi = \frac{z}{R_C} ,$$

$$Q = \xi^2 + (1+\rho)^2 ,$$

and

$$k = 2\sqrt{\frac{\rho}{Q}} .$$

The normalizing field B_0 in Eq. (1) is the field at the center of each circular loop:

$$B_0 = \frac{\mu_0 I_C}{2\pi R_C} . \tag{2}$$

The definition of B_0 involves the coil current I_C, a quantity that will be relevant in Sec. II.B. If a toroidal array of N current loops with minor radius R_C, major radius R_0, and equal angular separation $2\pi/N$ between two planes is defined by consecutive loops, the magnetic field vector generated by such array at an arbitrary point in space **p** would be given by

$$\frac{\mathbf{B}(\mathbf{p})}{B_0} = \sum_{i=1}^{N} \frac{\mathbf{B_i}(\mathbf{p})}{B_0} = \mathbf{F}(\mathbf{p}, R_0, R_c, N) \ . \tag{3}$$

The vector function **F** depends on the major radius R_0, the coil radius R_C, the number of coils N, and the point of evaluation **p**, with its coordinates referenced to the geometric center of the torus defined by the coils. The evaluation of this function involves application of the superposition principle to the magnetic field vector and a series of coordinate transformations that allow the use of Eq. (1) for the calculation of the magnetic field, followed by the transformation back to the global frame of reference. The details of such calculations have been documented elsewhere[9] and programmed in a computer code for the purposes of mapping the vacuum TF.

The use of Eq. (3) allows for the calculation of the TF and observes the degree of homogeneity in the field along the toroidal direction. For a fixed value of major radius and standing in the equatorial plane of the torus, the magnetic field magnitude along the toroidal angular direction can be found. Figure 2 shows the magnetic field, normalized to the maximum field produced by an array of a different number of current loops with R_C = 0.25 cm, along the toroidal direction. Curves are shown for both the center of the array (R_0 = 0.45 m) and near the outer surface of a hypothetical plasma column with a radius r_p = 0.15 m, such that $R = R_0 + r_p$ = 0.6 m. The ripple effect can be clearly observed along the toroidal direction since in the poloidal planes that lie between two toroidal coils the field is weaker, reaching a minimum in the poloidal plane that bisects the intercoil region. It is also clear that the effect is much larger as the calculation is done for a larger major radius coordinate since the separation between two adjacent loops increases with major radius. Given that an increase in the number of loops reduces the intercoil space, the oscillations in the field along the toroidal direction also go down as N is increased. From the information presented in Fig. 2, and considering that the vacuum chamber consists of four sectors, it was decided that the TF coil array should have 16 coils (4 coils per sector), based on easy access to the planned ports and keeping construction cost down while keeping the ripple low enough.

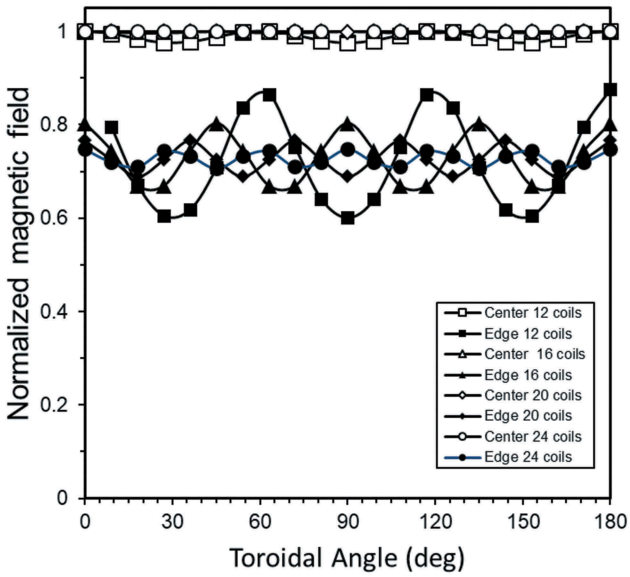

Fig. 2. Normalized magnetic field along the toroidal angle for a toroidal array of N circular coils with a major radius of 0.45 m and a minor radius of 0.25 m, shown at the center (solid) and at the edge (dashed) corresponding to a plasma radius of 0.15 cm. The ripple is clearly seen as oscillations in the field for low values of N and at the edge (larger value of R).

II.B. Magnetic Field Magnitude Requirements

Just like the number, shape, size, and position of the TF coils determine the shape of the toroidal magnetic field, the plasma current determines the magnitude of the required TF. To understand how this is the case, the starting point is recalling the definition of the safety factor[10]:

$$q(r) = \frac{2\pi}{\iota(r)} = \frac{r\ B_\phi}{R_p\ B_\theta} \ . \tag{4}$$

This quantity is a measure of the twist of the magnetic field resulting from the sum of the toroidal magnetic field B_ϕ (generated by the set of TF coils discussed in Sec. II.A) and the poloidal magnetic field B_θ (generated by the plasma current). It is a function of minor radius r, as can be seen from Eq. (4). Ampere's law gives the relationship between the poloidal field and the plasma current I_p, assuming purely toroidal current and $r \geq r_p$:

$$B_\theta(r) = \frac{\mu_0 I_p}{2\pi r} \ . \tag{5}$$

On the other hand, the combination of Eqs. (2) and (3) yields an expression for the TF:

$$B_\phi(r) = \frac{\mu_0 I_C}{2\pi R_C} |\mathbf{F}| \ . \tag{6}$$

Recall from Eq. (3) that **F** is a vector function that depends only on the number, shape, size, and position of the TF coils, as well as the coordinates of the point where the field is calculated. The substitution of Eqs. (5) and (6) in Eq. (4) evaluated at the plasma edge ($r = r_p$) yields

$$q(r_p) = \frac{r_p^2 I_C}{R_C R_p I_p} \left|\mathbf{F}(r_p)\right| . \tag{7}$$

The Kruskal-Shafranov stability limit addresses the case in which $q = 1$ at the plasma edge, for which case the confinement is unstable, so it is common practice in tokamaks to aim for a value of $q > 3$ at the plasma edge.[11] Setting Eq. (7) equal to 3 allows one to find the coil current I_C as a function of all geometrical parameters and the plasma with a current I_p:

$$I_C = \frac{3R_C R_p}{r_p^2 \left|\mathbf{F}(r_p)\right|} I_p . \tag{8}$$

Once all geometrical parameters for both the plasma and the TF coils are established, Eq. (8) gives the minimum coil current required to ensure stability as a function of plasma current.

II.C. Generation of Current Pulses Using Pulse-Forming Networks

In most small tokamaks, the current required to generate the toroidal magnetic field is achieved by the simple discharge of a capacitor bank.[12] Although simple, this strategy does not make optimal use of the energy storage infrastructure. Therefore, a different approach for current pulse shaping is suggested here: the use of a pulse-forming network (PFN). PFNs based on passive elements, named line-type PFNs, were key in the early days of radio, television, and radar[13] since they provided a robust method for generating high-current and high-voltage pulses. The generic diagram of a PFN is shown in Fig. 3, which shows a network of impedances in series parallel. Each of the branches on this array can be used to simulate a term in a Fourier series.

Once the plasma pulse length desired is specified, it is used for constructing a normalized symmetric trapezoidal pulse. The trapezoidal half-pulse is assumed to have a total width τ; it rises linearly to intensity 1 in a time $t = \alpha\tau$, remains at unity intensity until $t = \tau(1 - \alpha)$, and then goes back linearly to zero at $t = \tau$, as depicted in Fig. 4a. This normalized current pulse I^* can be expressed as a general Fourier series:

$$I^*(t) = \frac{I(t)}{I_{max}} a_0 + \sum_{k=1}^{\infty} (a_k \cos \omega_k t + b_k \sin \omega_k t) . \tag{9}$$

The pulse frequency ω_0 is given by π/τ, and ω_k is simply the frequency of the k'th harmonic $k\omega_0$. Some of the

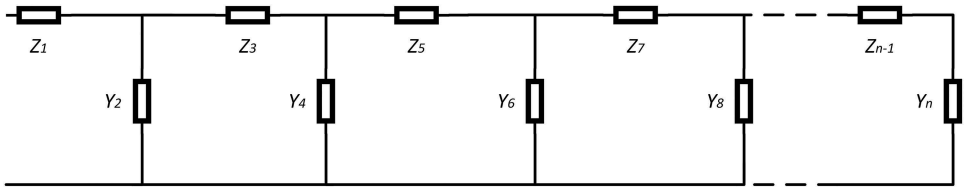

Fig. 3. A generic ladder PFN, comprising an array of impedances/admittances in series/parallel.

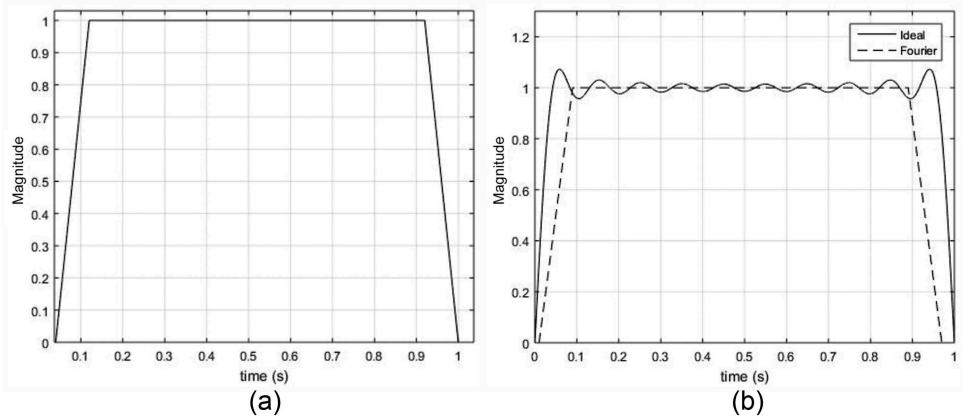

Fig. 4. (a) Ideal trapezoidal pulse showing the timing parameters and (b) comparison of the ideal trapezoidal pulse with a ten-term Fourier series.

coefficients in Eq. (9) can be dropped: All a_k coefficients are zero since the pulse is an odd function, and the b_k coefficients with k even are also zero due to the quarter-wave symmetry property of the trapezoid. The function describing the pulse is then given by

$$I^*(t) = \sum_{k\ odd}^{\infty} b_k \sin(\omega_k t)\ . \tag{10}$$

The Fourier coefficients are defined as

$$b_k = \frac{4\omega_0}{\pi} \int_0^{\pi/2\omega_0} I^*(t)\ \sin\omega_k t\ dt\ . \tag{11}$$

The function I^* can be specified piecewise to give the trapezoidal shape:

$$I^*(t) = \begin{cases} \frac{t}{\alpha\tau},\ 0 \le t \le \alpha\tau \\ 1,\ \alpha\tau \le t \le \tau(1-\alpha) \\ \frac{1}{\alpha}\left(1-\frac{t}{\tau}\right),\ \tau(1-\alpha) \le t \le \tau \end{cases}\ . \tag{12}$$

By substituting Eq. (12) in Eq. (11) and applying the quarter-wave symmetry condition, the Fourier coefficients are found to be

$$\begin{aligned} b_k &= \frac{4}{\tau}\left(\int_0^{\alpha\tau} \frac{t}{\alpha\tau}\ \sin\omega_k t\ dt + \int_{\alpha\tau}^{\tau/2} \sin\omega_k t\ dt\right) \\ &= \frac{2}{k^2\pi^2\alpha}\,\mathrm{sen}2k\alpha\pi\ . \end{aligned} \tag{13}$$

It is clear from Eq. (13) that the Fourier coefficients are only a function of the parameter α and that once the pulse geometry and that parameter are fixed, the Fourier coefficients do not change. Table II presents the values of the first ten Fourier coefficients, and Fig. 4b presents a comparison between the ideal trapezoidal pulse and the pulse generated by the ten-term Fourier series.

TABLE II

Design Parameters of the TPM-1U Tokamak

TPM-1U Design Parameters	
Major radius (m)	0.40
Minor radius (m)	0.15
Central magnetic field (T)	0.5 to 1.0
Plasma current (kA)	25 to 50
Central electron density (m^{-3})	1×10^{19}
Central electron temperature (eV)	300
Pulse time duration (ms)	10 to 30

The circuit shown in Fig. 5 can produce a trapezoidal current pulse built from a five-term Fourier series; the elements of that circuit are related to the Fourier coefficients by expressions (14a) and (14b):

$$C_k = \frac{b_k}{k\omega_0 Z_T} \tag{14a}$$

and

$$L_k = \frac{Z_T}{\omega_0 k b_k}\ . \tag{14b}$$

The total impedance Z_T is related to the capacitor charging voltage V_0 and the plateau value of the current $I_{\max}$ by

$$Z_T = \frac{V_0}{I_{max}}\ . \tag{15}$$

III. RESULTS

III.A. Determination of Size and Position to Minimize Ripple

Since the number of coils is already set to 16, it is now necessary to determine the size and position of the TF coils since those two parameters also determine the toroidal magnetic field shape. The TF ripple ψ is a good indicator of the TF homogeneity, and the recommendation for stable operation is to keep its value below 0.05 at the edge of the plasma column.[14] The definition used here for the TF ripple is

$$\psi = \frac{B_{\max} - B_{\min}}{B_{\max}}\ . \tag{16}$$

Consider two tori, one defined by the tokamak plasma column and another defined by the TF coil array. Naturally, these two tori have the same global geometrical center but different size parameters. Figure 6 shows a poloidal cross section to illustrate this fact, depicting a TF coil (with major radius R_0 and minor radius R_C) and the plasma column (with major radius R_p and minor radius r_p). The radial coil displacement ΔR is defined as

$$\Delta R = R_0 - R_p\ . \tag{17}$$

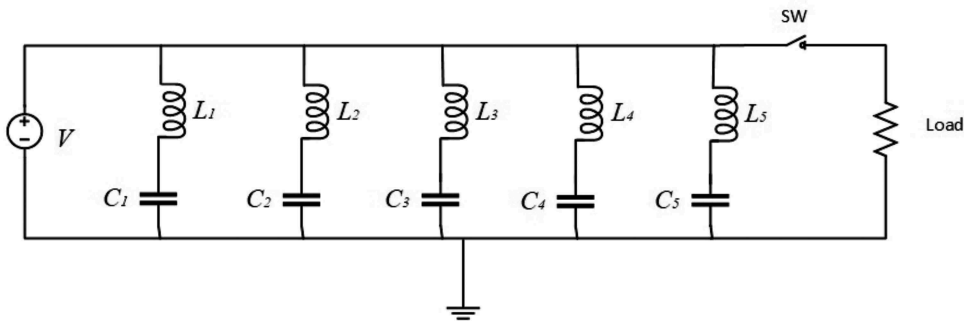

Fig. 5. The *LC* circuit used to generate a trapezoidal pulse. The values of the elements *L* and *C* on each branch are related to the shape parameters of the trapezoidal pulse.

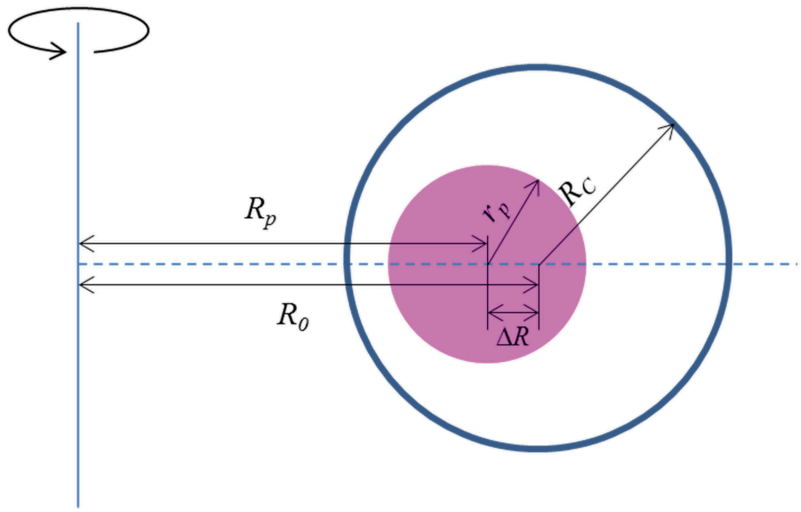

Fig. 6. Cross section of the tokamak showing the plasma column, the TF coil, and the relevant geometric parameters.

For the case of 16 coils and R_p = 0.45 m (defined by the existing vacuum vessel), it is important to quantify the ripple given the plasma column minor radius, the radial coil displacement, and the coil minor radius and then evaluate the ripple at the edge of the plasma ($R = R_p + r_p$). Figure 7 shows the ripple at the plasma edge as a function of the dimensionless radial coil displacement $\Delta R/R_C$ for the particular case of a plasma major radius of 0.45 m. Curves for different values of r_p/R_C are shown in Fig. 7 since the ripple is also a function of coil radius and plasma minor radius. The horizontal dotted line in Fig. 7 represents the upper limit of the ripple (0.05), and the mechanical restrictions for the shift values are also shown as dotted lines. The mechanical restrictions arise from the need of free space in the center of the tokamak to place the current transformer (that sets the minimum shift) and the fact that as soon as the coil hits the vacuum chamber, it cannot be shifted outward any farther (therefore setting the maximum shift). This means that the mechanically available region and the maximum allowable ripple bound the region of interest for the present design in Fig. 7.

Upon fixing the values for plasma major radius and minor radius, Fig. 7 gives the size and position of the coils that produce an acceptable ripple. Only coils with r_p/R_C values between 0.3 and 0.45 can be considered, and the minimum size coil is given by the largest value of r_p/R_C, corresponding to R_C = 0.222 m. To give a ripple below 5%, Fig. 7 indicates that the shift ΔR can be between 0.04 and 0.07 m. Rounding the coil radius value to 0.25 m, a comfortable number for manufacturing, and picking the midpoint radial displacement of 0.04 m, the value of the ripple finally obtained from Fig. 7 is 2.5%, which is half the maximum value.

Now that all the parameters of the coils have been established, Fig. 8 shows the normalized toroidal magnetic field at the outer equatorial edge

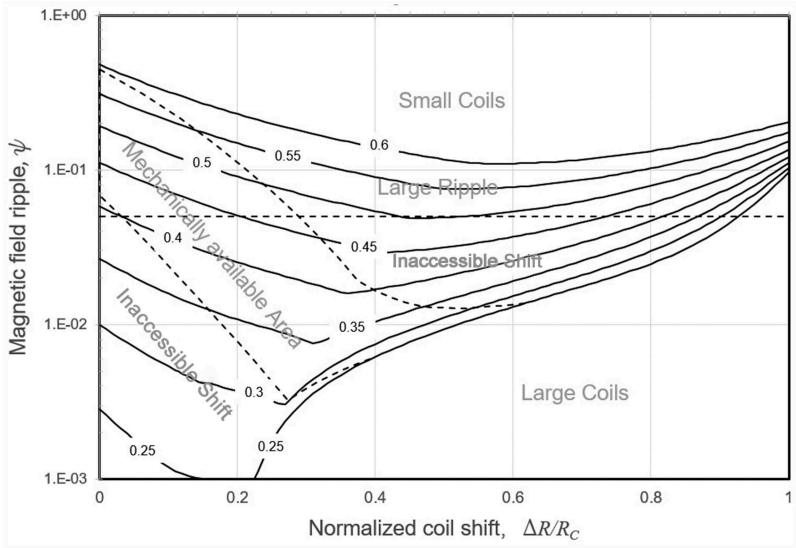

Fig. 7. Magnetic field ripple at the plasma edge (r_p = 0.1 m) as a function of the normalized center offset $\Delta R/R_C$ for a set of 16 coils. Curves shown are for different values of r_p/R_C, with dashed lines showing the boundaries of different regions.

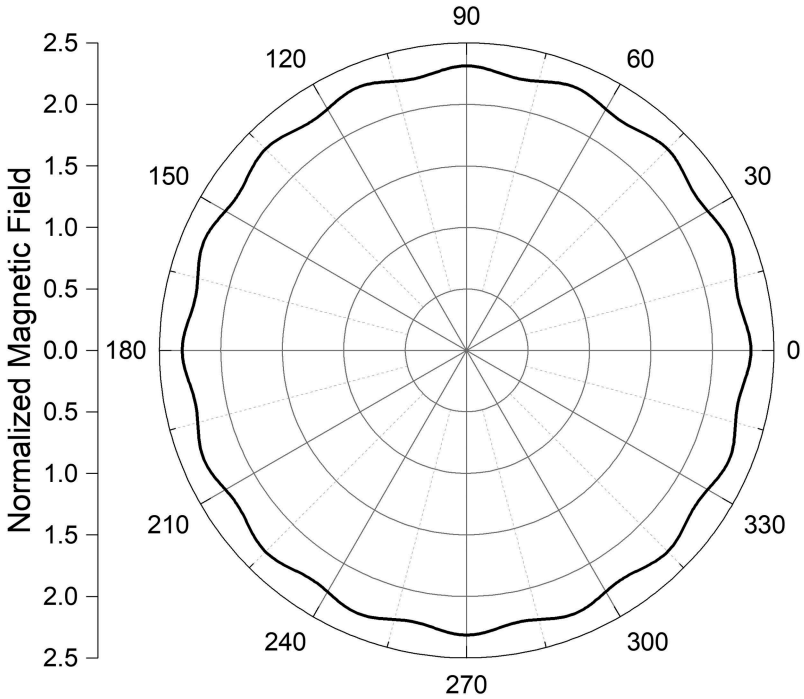

Fig. 8. Normalized toroidal magnetic field at the outer edge (R = 0.55 m) of a toroidal plasma column with R_p = 0.45 m and r_p = 0.1 m, surrounded by a toroidal array of 16 circular coils with R_C = 0.25 m and ΔR = 0.04 cm.

(R = 0.55 m) of a toroidal plasma column with R_p = 0.45 m and r_p = 0.1 m, surrounded by a toroidal array of 16 circular coils with R_C = 0.25 m and ΔR = 0.04 cm. The value is around 0.0025, as is predicted from Fig. 7. This is an indication that the number, size, and position of the coils are adequate for the operation of the TPM-1U tokamak. Table II summarizes the geometrical parameters for the plasma and the array of TF coils. The nontrivial parameter, the magnitude of the geometric factor $\mathbf{F}(r_p)$, which is necessary to calculate the coil current, is plotted versus toroidal angle in Fig. 8, and by using the geometric parameters already determined, Eq. (8) can be used to calculate the required coil current.

III.B. Required Current and Thermal Considerations

In Sec. II.C, all the geometrical parameters for the TPM-1U TF coil configuration were established (see Table II) to ensure a field ripple below 0.005 at the plasma edge, which helps avoid particle trapping and other instabilities. At this point, the numerical values of these parameters can be inserted in Eq. (8) to estimate the coil current required:

$$I_C \cong 15 I_p \ . \tag{18}$$

If the plasma current requirement is 50 kA, the current circulating in the coil needs to be 750 kA. Of course, if the coil is constructed by winding a conductor forming m layers of n turns each, then the current is scaled by a factor mn; however, the trade-off is that the size, weight, and resistance of the coil increase significantly. Consider for the coil construction, 4 AWG solid magnet wire [with circular cross section of 21.15 mm^2, resistance of 0.8152 mΩ/m, and weight of 184.5 kg/km (Ref. 15)] and a coil winding of eight layers with eight turns each. This gives a coil current conduction area of 13.53 cm^2, and the current on each turn is 12 kA. This means that a square coil conduction cross section of 4 × 4 cm is sufficient to accommodate the 64 turns; each coil would require a conductor length of 110 m, giving a resistance of 0.09 Ω and a mass of 20 kg/coil. The power dissipated by the current circulation on each coil is 13 MW, which in the 30 ms of the shot translates into an energy of 390 kJ. Considering the copper mass present in the coil, the deposition of this energy in the coil causes an increase of 50°C in its temperature with no dissipation. Repeating the calculation for a plasma current of 25 kA (50% of the design value), the increase is only 12.5°C (25% of the previously calculated value) due to the quadratic relationship of the deposited power with coil current.

III.C. Current Pulse Generation for the TF System

The ATP software was used to simulate the electric current transient produced by the PFN shown in Fig. 5, referred to in the literature as a Type C PFN (Ref. 13). The elements of the circuit are calculated using Eq. (14), considering a pulse plateau width of 30 ms, unity impedance, and the first five values from Table III. A comparison among the ideal pulse and the pulse predicted by the positive five-term Fourier series, the pulse obtained from the ATP simulation, is shown in Fig. 9, where it can be clearly seen that the circuit accomplishes the task of keeping the current at a flat value during the desired time interval, with a slight reduction of the time in the case of the simulated pulse. The modeled pulse deviates during the rampdown of the current, but this portion of the pulse has little relevance in the operation of the machine.

TABLE III

First Ten Fourier Coefficients to Give the Trapezoidal Pulse Shown in Fig. 4a

n	b_n
1	1.2266
3	0.2965
5	0.0764
7	−0.0086
9	−0.0297
11	−0.0199
13	−0.0025
15	0.0085
17	0.0092
19	0.0034

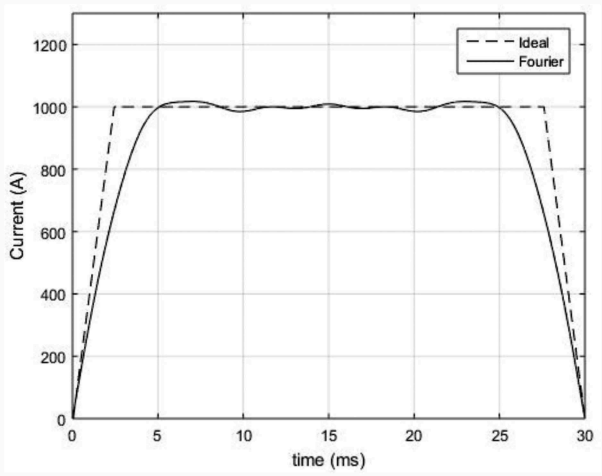

Fig. 9. Comparison among the ideal trapezoidal pulse, the five positive term Fourier series approximation, and the current calculated with the ATP software for the circuit of Fig. 5 and the circuit element values of Table III.

The Type C network can be modified to generate an equivalent circuit where all the stages have the same capacitance (a circuit topology named Type E network), which is something that facilitates the construction of the PFN. This is accomplished by recursive application of the Cauer impedance theorem and obtaining a network with equivalent impedance and the same resonance characteristics, but with equal capacitance on each stage.[13] The circuit for the Type E network is shown in Fig. 10a. Following an approach already reported in the literature[16]

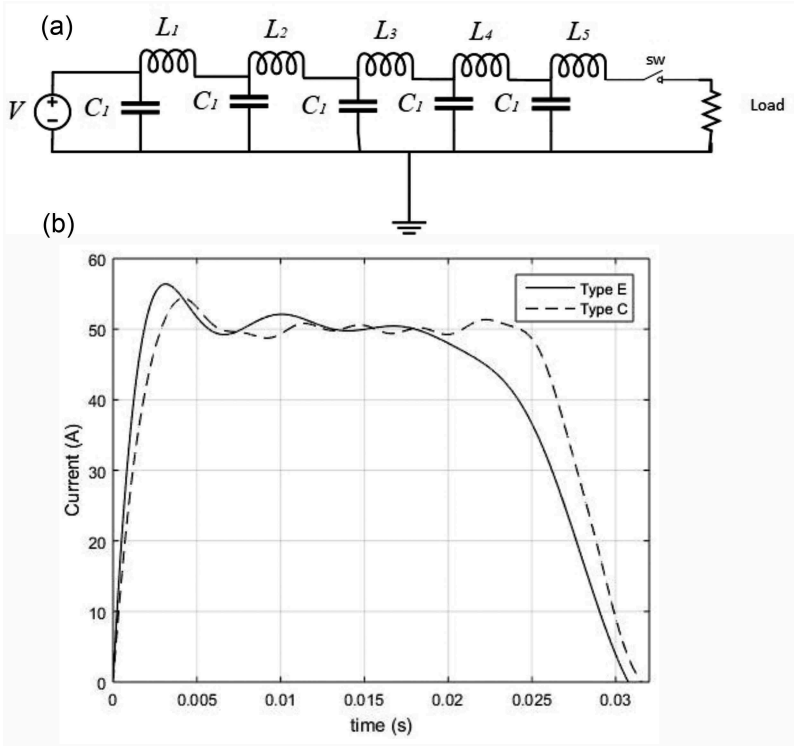

Fig. 10. (a) Circuit topologies and (b) comparison of the current pulses obtained with ATP simulations for Type C (solid) and Type E (dashed) PFNs with circuit elements given by Tables III and IV, respectively.

TABLE IV

Values for the Circuit Elements in Type C and Type E Networks with a 1-Ω Resistive Load and 30-ms Pulse Length

Stage	Capacitor (μF)	Inductor (mH)
Type C Network Values		
1	11833.488329	7.7060172575
2	1046.2845959	9.6839028349
3	218.86987774	16.665439067
4	28.238634189	65.902667947
5	3.257995306	96.848849752
Type E Network Values		
1	2754.3	2.5305
2	2754.3	2.1642
3	2754.3	2.0541
4	2754.3	1.9861
5	2754.3	2.2192

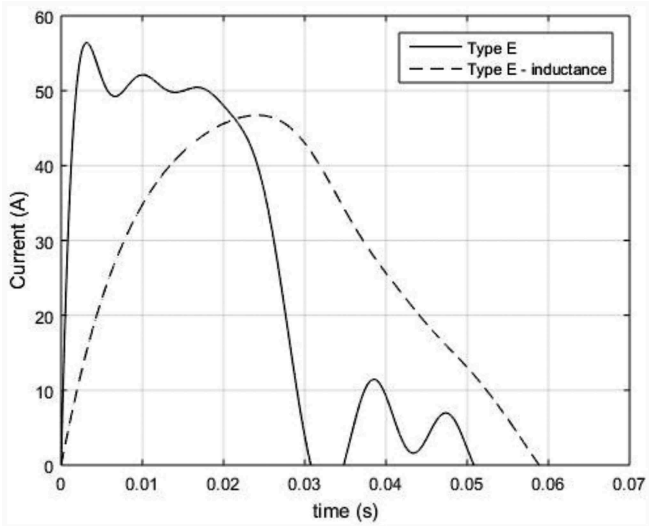

Fig. 11. Simulation of current pulses for the Type E network with a resistive load of 1 Ω (solid) and the same network with an inductive load of 16 mH (dashed).

for converting from Type C (Fig. 5) to Type E (Fig. 10a) topologies, the values for the circuit elements in both the Type C and Type E networks are presented in Table IV, and the comparison of the pulse shapes is shown in Fig. 10b.

One last aspect of the power delivery system to be discussed here is the case of highly inductive loads, such as the TF coil array of the TPM-1U tokamak. Figure 11 shows the comparison of ATP simulations between the response of the Type E network with a resistive 1-Ω load constructed with the values of Table IV and the same network connected to a purely inductive 16-mH load. Clearly, the inductive character of the load completely

deforms the intended pulse. Two strategies can be used in order to solve this problem: (1) use a low-resistance 1:1 transformer to magnetically couple the PFN to the coil array and (2) tune the PFN to deal with an inductive load by design. Only the second approach will be discussed here since it builds on previously discussed theory.

The details of the strategy to attack the problem is outlined somewhere else,[17] but in general it consists of treating the inductive load as a voltage source that generates an opposing current. Consider the exact same circuit as Fig. 5 but with an inductor L_0 connected to the load. By Kirchoff's current law, the current discharged by each of the j'th stages in the PFN should satisfy

$$L_0 \frac{d^2 I}{dt^2} + L_j \frac{d^2 I_j}{dt^2} + \frac{I_j}{C_j} = 0 \ , \tag{19}$$

where I_j is the contribution of the j'th stage to the total current that circulates on the load I^* still given by a Fourier expansion, Eq. (10), after normalization. The normalized voltage drop V^* across the inductive load is given by

$$V^* = -\frac{L_0}{Z_T}\frac{dI^*}{dt} = -\frac{L_0}{Z_T}\sum_{k\ odd}^{\infty} \omega_k b_k \cos(\omega_k t) \ . \tag{20}$$

The voltage at the load and the terminals of each leg j should match. Hence, the current contribution from the opposing inductive load for each of the harmonic components k is given by

$$L_j \frac{dI^*_{j,k}}{dt} + \frac{1}{C_j}\int I^*_{j,k} dt = -\frac{L_0}{Z_T}\omega_k b_k \cos(\omega_k t) \ . \tag{21a}$$

To get rid of the integral, the derivative of Eq. (22) is taken:

$$L_j \frac{d^2 I^*_{j,k}}{dt^2} + \frac{I^*_{j,k}}{C_j} = -\frac{L_0}{Z_T}\omega_k b_k \cos(\omega_k t) \ . \tag{21b}$$

Equation (21b) needs to be solved, subject to the initial conditions of zero opposing current and known initial charging voltage. The application of these boundary conditions yields the following solution:

$$I^*_{j,k} = -\frac{L_0 b_k}{Z_T Z_{j,k}}\left[\omega_k \sin(\omega_k t) - \omega_j \sin\left(\omega_j t\right)\right]$$

and

$$Z_{j,k} = \omega_k L_j - \frac{1}{\omega_k C_j} \ . \tag{22}$$

On the other hand, the current produced by the discharge of the capacitors C_j on each branch is given by

$$I^*_j = \frac{Z_T}{\omega_j L_j}\sin\left(\omega_j t\right) \ . \tag{23}$$

The total normalized current circulating on the load is therefore given by

$$\sum_k b_k \sin(\omega_k t) = \sum_j \left[\frac{Z_T}{\omega_j L_j}\sin\left(\omega_j t\right) - \frac{L_0}{Z_T} \times \sum_k \frac{b_k}{Z_{j,k}}\left[\omega_k \sin(\omega_k t) - \omega_j \sin\left(\omega_j t\right)\right]\right] . \tag{24}$$

Making all coefficients for the different frequency components equal on both sides of Eq. (24) and expressing the branch impedances $Z_{j,k}$ in terms of the frequencies ω_j and ω_k yield two sets of equations:

$$1 = -\frac{L_0 \omega_k}{Z_T}\sum_j \frac{C_j}{\left(\frac{\omega_k}{\omega_j}\right)^2 - 1} \tag{25a}$$

and

$$0 = \frac{Z_T}{L_0} + \sum_k \frac{b_k \omega_k}{\left(\frac{\omega_k}{\omega_j}\right)^2 - 1} \ . \tag{25b}$$

The parameters Z_T, L_0, ω_k, and b_k are prescribed by the load inductance, the charging voltage, the desired plateau current value, and the pulse shape; therefore, Eq. (25) needs to be solved for ω_j and C_j. A good strategy is to find the n roots of the polynomial Eq. (25b) and find all the ω_j's, and then use these values to solve the linear system of Eq. (25a) for all C_j's. Once all ω_j's and C_j's are known, values for all L_j's are easy to calculate. Given the parameters from Table III, unity total impedance and a 16-mH inductive load, the circuit values for the compensated Type C network are presented in Table V. The pulse shape corresponding to these circuit values was calculated with ATP, and it is shown in Fig. 12, where it is clear that the circuit element calculation strategy outlined above has succeeded in obtaining

TABLE V

Values for the Circuit Elements in a Type C Network with a 16-mH Inductive Load and 30-ms Pulse Length

Stage	Capacitor (μF)	Inductor (mH)
1	1390	48.1
2	159	46.6
3	60.5	43.7
4	33.2	39.2
5	157	4.18

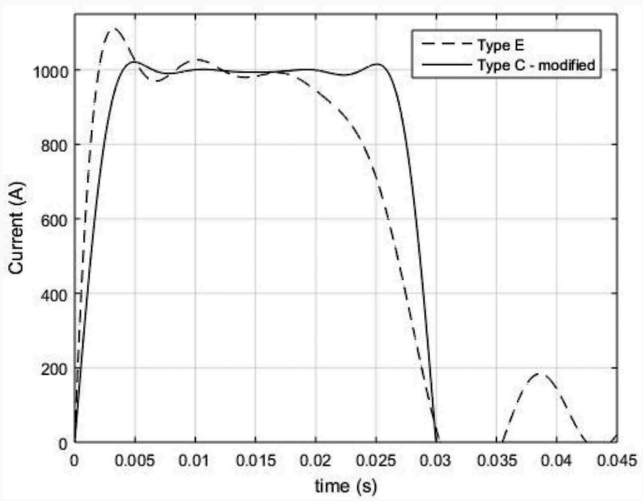

Fig. 12. Current pulse generated by a Type C PFN with a 16-mH inductive load constructed with the values from Table V (solid line), compared with the Type E network with a resistive load (dashed).

a pulse with the desired shape. The transformation of this compensated Type C network to a Type E is not trivial, and the discussion of such transformation will be the subject of a future paper.

IV. CONCLUSIONS

The TF coil for the TPM-1U tokamak, a machine being planned at CICATA Querétaro, has been designed considering requirements regarding TF ripple, maximum plasma current to be confined, and pulse length. It has been found that a set of 16 circular coils with a radius of 0.25 m, placed with a center offset of 4 cm outward with respect to the plasma column center, is sufficient to generate a TF with a maximum ripple below 5% at the plasma edge, ensuring stability of operation. If the maximum plasma current expected in the plasma is 50 kA, a coil with eight layers of eight turns each would require the circulation of 12 kA. The circulation of that current would mean a temperature increase of 50°C in the coil, so provisions for air cooling will be necessary. The 30-ms pulse of 12 kA can be achieved by a Type C or Type E PFN, which can generate a trapezoidal pulse for the case of a purely resistive load. The Type E network with five stages requires capacitors of 3000 μF with a charging voltage of 6 kV. Currently, values for a Type C network able to produce the desired pulse for a 16-mH inductive load have been obtained successfully, but the analysis to obtain a Type E network for operation with an inductive load is ongoing, and those results will be the focus of a follow-up paper.

Acknowledgment

The authors wish to thank C. Rose from Los Alamos National Laboratory for helpful discussion regarding methods for the transformation of PFNs from Type C to Type E.

ORCID

M. Nieto-Pérez http://orcid.org/0000-0001-6600-9786

References

1. M. VÁZQUEZ REYNA, *El Tokamak TPM – 1 Parte I*, Instituto Nacional de Investigaciones Nucleares – Escuela Superior de Ingeniería Mecánica y Eléctrica IPN (1983) (in Spanish).
2. S. MÜLLER, "Turbulence in Basic Toroidal Plasmas," PhD Thesis, EPFL, Switzerland (2006).
3. C. A. F. VARANDAS, "Engineering Aspects of the Tokamak ISTTOK," *Fusion Technol.*, **29**, *1*, 105 (1996); https://doi.org/10.13182/FST96-A30660.
4. J. BROTÁNKOVÁ, "Study of High Temperature Plasma in Tokamak-Like Experimental Devices," PhD Thesis, Charles University, Prague (2009).
5. R. ALIPOUR et al., "Investigation on the Effect of Pressure on Turbulent Transports of the IR-T1 Tokamak Plasma," *Eur. Phys. J. D*, **71**, 60 (2017); https://doi.org/10.1140/epjd/e2017-70563-6.
6. W. ZHANG et al., "Improved Confinement and Edge Plasma Fluctuations in the STOR-M Tokamak," *Phys. Fluids B*, **4**, 3277 (1992); https://doi.org/10.1063/1.860383.
7. F. CEBALLOS-SOTO, M. NIETO-PEREZ, and G. RAMOS, "Design of a Pulse Transformer for the Ohmic Heating System of a Small Tokamak," *Fusion Eng. Des.*, **121**, 325 (2017); https://doi.org/10.1016/j.fusengdes.2017.05.018.

8. D. BRUCE MONTGOMERY, *Solenoid Magnet Design*, Wiley Interscience, New York (1969).

9. D. M. VENTURA-OVALLE, "Cálculo de las fuerzas electromagnéticas en las bobinas toroidales del Tokamak TPM-1U," MS Thesis, Instituto Politécnico Nacional (2016).

10. J. SHEFFIELD, "The Physics of Magnetic Fusion Reactors," *Rev. Mod. Phys.*, **66**, *3*, 1015 (1994); https://doi.org/10.1103/RevModPhys.66.1015.

11. J. P. FREIDBERG and A. HAAS, "Kink Instabilities in a High-Beta Tokamak," *Phys. Fluids*, **16**, *11*, 1909 (1973); https://doi.org/10.1063/1.1694233.

12. M. GRYAZNEVICH et al., "First Results from Tests of High Temperature Superconductor Magnets on Tokamak," *Proc. 24th IAEA Fusion Energy Conf.*, San Diego, California, October 2012, International Atomic Energy Agency (2012).

13. G. N. GLASOE and J. V. LEBACQZ, *Pulse Generators*, McGraw-Hill (1948).

14. N. A. UCKAN, T. UCKAN, and J. R. MOORE, "Calculation of Magnetic Field Ripple Effects in Circular and Noncircular Tokamak," ORNL/TM-5603, Oak Ridge National Laboratory (1976).

15. "Magnet Wire/Winding Wire Engineering Data Handbook," Superior Essex; https://www.superioressex.com/uploadedFiles/Magnet_Wire_and_Distribution/North_America/Magnet_Wire_-_Winding_Wire/EngData_book_linked.pdf (current as of June 5, 2018).

16. C. R. ROSE, "Type E Pulse Forming Network: Theory and Synthesis," *Proc. IEEE Pulsed Power Conf.*, Austin, Texas, May 31–June 4, 2015, IEEE (2015).

17. D. RIHNEY, L. KRAUS, and H. MALAMUD, "Synthesis of Current Waveforms by Type C Networks," Plasma Propulsion Laboratory Republic Aviation Corporation (1961).